IEEE Access
Multidisciplinary | Rapid Review | Open Access Journal

Received June 3, 2019, accepted June 26, 2019, date of publication July 23, 2019, date of current version August 9, 2019.

Digital Object Identifier 10.1109/ACCESS.2019.2929237

Integrating Five Feature Types Extracted From Ultrasonograms to Improve the Prediction of Thyroid Papillary Carcinoma

RENXIANG ZHU[1], ZHONGYU WANG[1], YIFAN ZHANG[1], BINGXIN YU[2], MINGRAN QI[1], XIN FENG[1], CHENJUN WU[1], YUXUAN CUI[1], LAN HUANG[3], FAN LI[2], AND FENGFENG ZHOU[1]

[1]BioKnow Health Informatics Laboratory Key Laboratory of Symbolic Computation and Knowledge Engineering, College of Computer Science and Technology, Ministry of Education, Jilin University, Changchun 130012, China

[2]The Key Laboratory of Zoonosis, Department of Pathogenobiology, College of Basic Medicine, Ministry of Education of China, Jilin University, Changchun 130021, China

[3]Key Laboratory of Symbolic Computation and Knowledge Engineering, College of Computer Science and Technology, Ministry of Education, Jilin University, Changchun 130012, China

Corresponding authors: Fengfeng Zhou (ffzhou@jlu.edu.cn) and Bingxin Yu (148040196@qq.com)

This work was supported in part by the Strategic Priority Research Program of the Chinese Academy of Sciences under Grant XDB13040400, in part by the Jilin Provincial Key Laboratory of Big Data Intelligent Computing under Grant 20180622002JC, in part by the Education Department of Jilin Province under Grant JJKH20180145KJ, in part by the startup grant of Jilin University, in part by the Bioknow MedAI Institute under Grant BMCPP-2018-001, in part by the High Performance Computing Center of Jilin University, and in part by the Fundamental Research Funds for the Central Universities, JLU.

ABSTRACT Ultrasonogram is one of the main techniques for the non-invasive observation and the diagnosis of the thyroid gland. And, the thyroid papillary carcinoma (TPC) was usually diagnosed during the regular examination of the thyroid gland. The current diagnosis guideline heavily replies on the experienced clinical endoscopists. This paper comprehensively evaluated four classification algorithms and five image feature extraction algorithms for the TPC diagnosis problem. Our data demonstrated that the Hessian features extracted from the transverse ultrasonograms performed better than those from the longitudinal view. The best model (Acc = 0.9949) was achieved by the seven-layer shallow neural network with the LBP and Hessian features extracted from both the longitudinal and transverse views of the ultrasonograms.

INDEX TERMS Thyroid pappilary carcinoma (TPC), transverse ultrasonogram, longitudinal ultrasonogram, feature extraction, deep neural network.

I. INTRODUCTION

Thyroid gland is an endocrine organ in the front of the neck and secretes essential hormones for metabolisms [1] and protein synthesis [2]. Thyroid hormones may be produced at the amount exceeding the regular body needs, which may be caused by various factors including the autoimmune disorder Graves' disease [3], [4]. Thyroid cancer has the symptoms of lumps in the neck and may be caused by the radiation exposures and genetic risks [5]. Thyroid papillary carcinoma (TPC) is the major subtype of thyroid cancer and has very good prognosis [6].

TPC has no symptoms at the early stages [7], [8] and was usually diagnosed incidentally during other regular health checkup by ultrasonogram [9], [10]. As high as 7% of American adults have thyroid palpable nodules [11], and about 10% of these thyroid nodules may be malignant [12], [13]. So the current clinical thyroid guideline recommends all patients with thyroid nodules to take ultrasonogram [14]. A clinician may decide whether to proceed with further tests after integrating the clinical factors and the ultrasonogram results [15]. Finally the guideline suggests a fine-needle aspiration biopsy with cytology (FNAB) to determine whether to do the thyroid surgery.

Various types of features were extracted from the ultrasonogram images and machine learning algorithms were utilized to build the predictive models for clinical phenotypes. The histogram of oriented gradient (HOG) features extracted from the ultrasonograms was utilized to predict the pediatric abnormalities of the kidney and urinary tract and achieved

The associate editor coordinating the review of this manuscript and approving it for publication was Haiyong Zheng.

the prediction accuracies between 81% and 87% [16]. Local binary patterns (LBP) was a popular algorithm to describe the image texture patterns and was utilized to detect breast lesion [17], [18]. The recent study demonstrated that the integration of multiple image feature types may improve the diagnosis accuracy of breast cancer [18]. A number of other feature extraction algorithms were also explored for their applicability in ultrasonogram-based disease predictions, e.g., the gray-level co-occurrence matrix (GLCM) [19], the Hessian matrix (Hessian) [20] and the Canny operator [20], etc. The recent state-of-the-art TPC prediction study proposed to use the convolutional neural network (CNN) to detect TPC based on the ultrasonogram images and achieved 93.5% in the TPC detection accuracy [21].

This study hypothesized that the ultrasonogram based TPC prediction model may be improved by integrating various feature types. We firstly described the ultrasonogram images in the following types of features, i.e., histogram of oriented gradient (HOG) [16], local binary patterns (LBP) [17], [18], gray-level co-occurrence matrix (GLCM) [19], the Hessian matrix (Hessian) [20] and the Canny operator [20]. Then we evaluated how these types of features were integrated to improve the ultrasonogram based TPC prediction model.

II. MATERIALS AND METHODS

A. DATA SET

This study established a cohort of thyroid papillary carcinoma (TPC) patients and their controls in the China-Japan Union Hospital of the Jilin University. Patients and controls were diagnosed by the experienced clinicians and the ultrasonograms were collected as JPG images. Each participant has the transverse and longitudinal ultrasonograms captured according to the guidelines [22]. This cohort has 114 TPC patients and 59 controls. This study was approved by the IRB committee of the China-Japan Union Hospital of the Jilin University. Each participant signed his or her informed consent form. After removing the personal information and clinical annotations, a rectangle of 730 × 420 pixels in size was extracted to contain the maximal ultrasonogram data.

B. PROBLEM MODEL AND PERFORMANCE MEASUREMENTS

A binary classification problem between TPC and control ultrasonograms was investigated in this study. A TPC patient was a positive sample, and there were P positive samples. While a control participant was a negative sample and the number of negative samples was N.

The binary prediction model was evaluated for its sensitivity (Sn), specificity (Sp) and accuracy (Acc). The numbers of correctly and incorrectly predicted positive samples were denoted as True Positive (TP) and False Negative (FN). And the sensitivity was defined as the percentage of correctly predicted positive samples, i.e., $Sn = TP/(TP + FN) = TP/P$. The specificity was defined as the percentage of correctly predicted negative samples, i.e., $Sp = TN/(TN + FP) = TN/N$, where TN (true negative) and FP (false positive) were the numbers of correctly and incorrectly predicted negative samples, respectively. The overall prediction accuracy was defined as $Acc = (TP + TN)/(TP + FN + TN + FP) = (TP + TN)/(P + N)$.

The Matthews' correlation coefficient has been widely used to evaluate biomedical prediction models based on protein sequences [23], small molecules [24] and images [25]. It was defined as $MCC = (TP \times TN\text{-}FP \times FN)/\mathrm{sqrt}((TP + FP) \times (TP + FN) \times (TN + FP) \times (TN + FN))$, where $\mathrm{sqrt}(x)$ was the squared root of x.

All the models were run by 5-fold cross validation and the model performances were calculated over 20 random runs. Three popular classifiers were evaluated on the binary classification problem. The classifier Gaussian naïve Bayes (NBayes) was utilized to build the binary prediction model [26], [27]. K nearest neighbor (KNN) algorithm was a simple but powerful classifier that relied on the definition of the inter-sample distance [28], [29]. The support vector machine (SVM) was another widely-used classifier and has been used in various types of applications, e.g., genomics [30] and fMRI imaging data [31]. The SVM model with the linear kernel was utilized in this study.

C. FEATURE EXTRACTION ALGORITHMS

Five popular types of features were extracted from an ultrasonogram image. Due to the personal heterogeneity in sizes and lesion locations, thyroid ultrasonograms of two persons cannot be directly compared. The statistical and other types of features were usually calculated from an image and a comparative modeling was then carried out among these features [32], [33].

The histogram of oriented gradients (HOG) algorithm has been widely applied for the object detection [34], [35]. The gradient features generated by HOG were also successfully applied to predict lung cancers [36].

The local binary patterns (LBP) exhibits the inherent characteristics of rotation-invariance and image texture description [37], [38]. LBP was initially proposed as a special case of the Texture Spectrum model [39], [40] and has been widely used to discriminate among different types of textures [41]–[43]. A major improvement may be achieved if the LBP features were combined with the HOG features to describe the image textures [44]. LBP has also been successfully applied to the problem of background subtraction [45].

The gray-level co-occurrence matrix (GLCM) describes the co-occurring gray-scale values in an image and the calculated spatial inter-pixel relationships were widely used in medical image analysis [46]–[48]. Integration of GLCM and LBP features may improve the coronary plague detection based on the intravascular ultrasound images [49] and the stroke detection based on the skull CT images [50].

Hessian matrix (Hessian) consists of the second-order partial derivatives of a scalar-value function, and describes a multi-variate function's local curvatures [ref]. A convex function has a positive semi-definite Hessian matrix and may

easily derive a local optimality [51]. Hessian matrix was used to quantitatively describe the vascular structures [52] and the microcalcification clusters [53].

The Canny operator (Canny) with appropriate thresholds was widely used to detect the boundaries in images [54]. The thresholds need to be carefully chosen with adaptive rules [55], and the Otsu algorithm performs the best in most cases [55].

D. FEATURE SELECTION BY GRADIENT BOOSTING DECISION TREE

A feature selection algorithm may select phenotype-associated features and exclude redundant features [56]. A gradient boosting decision tree (GBDT) algorithm builds an ensemble of multiple weak regression model [57]. GBDT iteratively improves weak learners with smaller differences between the predicted phenotypes and the real ones, and is used to rank target objects in many cases, e.g., the web search engines [58]. GBDT returns the importance factor for each feature, and the features with importance no smaller than a user-defined threshold will be selected for further analysis. The default threshold was set to 0.005.

E. IMPLEMENTATION

This study was carried out using the Python version 3.6 programming environment. The machine learning packages were sklearn version 0.20.3 and GBDT was implemented in sklearn.ensemble. Deep learning algorithms were implemented in keras version 2.2.4 and tensorflow version 1.12.0.

All the experiments were executed in an Inspur Gene Server G100 with 256GB memory, 28 Intel Xeon® CPU cores (2.4GHz), and 26 TB hard disk.

III. RESULTS AND DISCUSSION

A. EVALUATION OF FIVE FEATURE EXTRACTION ALGORITHMS ON THE LONGITUDINAL ULTRASONOGRAMS

This study kept the top-ranked 20 features of each feature type for further evaluation. GLCM extracted 64 features from a given image while all the other four algorithms generated over 300 thousand features. In order to integrate these five feature types by a similar number of features, each feature type was evaluated for the individual feature's discriminative power by t-test and the top-ranked 20 features with the smallest Pvalues were kept for further analysis.

The five feature types demonstrated different averaged values and standard deviations between the TPC samples and the controls, as illustrated by Figure 1. Hessian and LBP generated features with the top two largest averaged values. And the Canny features have a small averaged value and a relatively large standard deviation.

The prediction models were built using three popular classifiers, i.e., NBayes, KNN and SVM. Five types of feature extraction algorithms were evaluated, i.e., HOG, LBP, GLCM, Hessian and Canny, on the longitudinal ultrasonogram images.

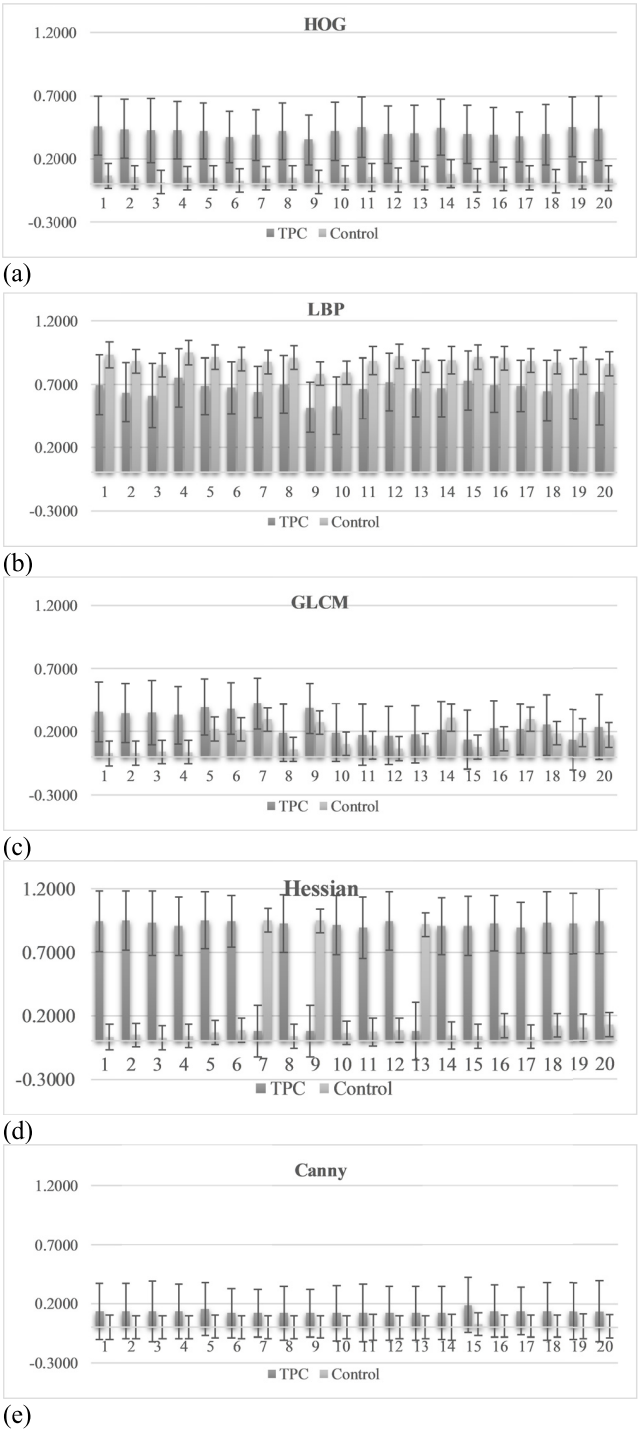

FIGURE 1. Average and standard deviation values of the top-ranked 20 features extracted by each of the five feature extraction algorithms. (a) HOG, (b) LBP, (c) GLCM, (d) Hessian, and (e) Canny.

Five feature extraction algorithms were evaluated for their performances of predicting TPC samples using the longitudinal ultrasonograms, as shown in Figure 2. The feature type Hessian achieved the best averaged prediction accuracy

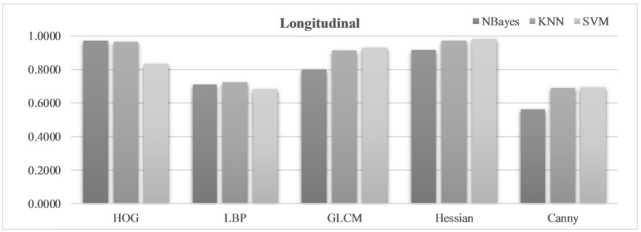

FIGURE 2. Comparison of five feature extraction algorithms on the longitudinal ultrasonograms.

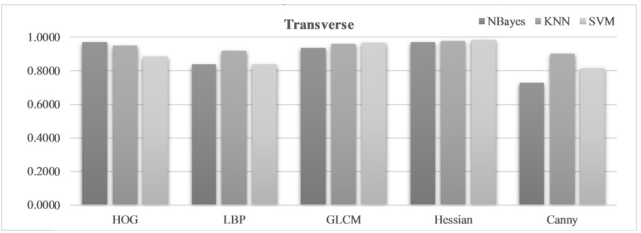

FIGURE 3. Comparison of five feature extraction algorithms on the transverse ultrasonograms.

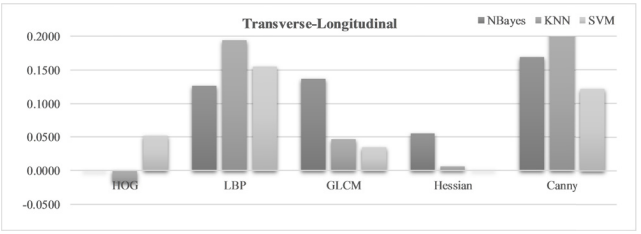

FIGURE 4. TPC prediction improvements using the transverse ultrasonograms compared with the longitudinal ones.

0.9561. And the second best feature type HOG achieved 0.9232. Figure 2 (a) demonstrated that the classifier SVM performed the best on the Hessian features (Acc = 0.9825). The next best prediction model was established by the classifier NBayes on the feature types HOG (Acc = 0.9717). The next two best prediction models were achieved by the classifier KNN on the two feature types Hessian (Acc = 0.9697) and HOG (Acc = 0.9654), respectively. All the other models didn't achieve Acc better than 95%.

The classifier KNN performed the best averaged prediction accuracy 0.8521 among the three utilized classifiers. Although the maximal prediction accuracy 0.9825 was achieved by the classifier SVM on the Hessian features, KNN's best prediction accuracy 0.9697 on the Hessian features was only 0.0128 smaller than the maximal accuracy (Acc = 0.9825). Zhang, H et al., confirmed the observation that the classifier KNN usually outperformed two popular classifiers SVM and NBayes in most cases [59].

B. EVALUATION OF FIVE FEATURE EXTRACTION ALGORITHMS ON THE TRANSVERSE ULTRASONOGRAMS

The prediction models were built using three popular classifiers, i.e., NBayes, KNN and SVM. Five types of feature extraction algorithms were evaluated, i.e., HOG, LBP, GLCM, Hessian and Canny, on the transverse ultrasonogram images.

The Hessian features demonstrated better discrimination powers between the TPC samples and controls using the transverse ultrasonogram, as shown in Figure 3. All the top three TPC prediction accuracies 0.9828, 0.9762 and 0.9717 were achieved on the same feature type (Hessian) by the classifiers SVM, KNN and NBayes, respectively. KNN performed the best on the transverse ultrasonograms, with at least 0.9000 in the TPC prediction accuracy on all the five feature types. Its averaged prediction accuracy was 0.9410, much better than that (Acc = 0.8893) of NBayes.

C. COMPARISON BETWEEN THE LONGITUDINAL AND TRANSVERSE ULTRASONOGRAMS

The prediction models were built using three popular classifiers, i.e., NBayes, KNN and SVM. Five types of feature extraction algorithms were evaluated, i.e., HOG, LBP, GLCM, Hessian and Canny, on the longitudinal and transverse ultrasonogram images. The vertical axis was the accuracy difference of a classifier on a feature type between the transverse and longitudinal ultrasonograms.

The prediction models using the transverse ultrasonograms generated better or equal accuracies compared with the longitudinal ones in most cases, as shown in Figure 4. The only exception was the feature type HOG, where the models using the transverse ultrasonograms performed slightly worse than the longitudinal ones. The prediction accuracies were decreased no more than 0.0200 for all the three classifiers. The averaged prediction accuracy improvements were similar for all the three classifiers SVM (0.0729), NBayes (0.0977) and KNN (0.0888), respectively. So overall, the transverse ultrasonogram provides better information for the TPC prediction using the classic machine learning algorithms.

D. CLASSIFICATION USING A DEEP LEARNING NETWORK

(a) The architecture of the classic deep learning network, LeNet-5. (b) Classification accuracies of LeNet-5 using different image features. The vertical axis was the classification accuracy.

In additional to the classic classification algorithms, this study further evaluated how a convolutional neural network performed on the dataset, as shown in Figure 5 (a). The deep neural network LeNet-5 was utilized in this study [60].

Figure 5 (b) illustrated that LeNet-5 didn't outperform the classic classifiers. LeNet-5 achieved the best accuracy 0.9482 on the GLCM features of the longitudinal view, which was worse than the best model of a classic algorithm (SVM, Acc = 0.9828) on the Hessian features, as shown in Figure 3. All the other feature types didn't achieve accuracies better than 0.7000. This may be due to the limited number of images for training LeNet-5. Another popular deep learning

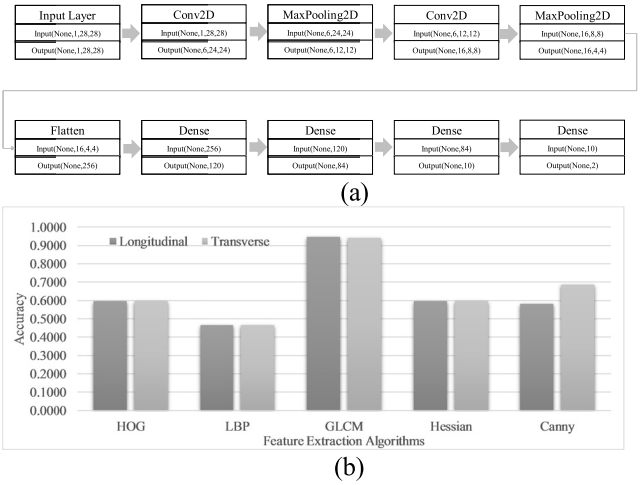

FIGURE 5. Deep learning network based classification.

framework AlexNet was also evaluated for our problem [61]. AlexNet performed similarly well with the previous model but still only achieved prediction accuracies less than 0.7000. So the two popular deep learning classifiers didn't outperform the classic machine learning algorithms.

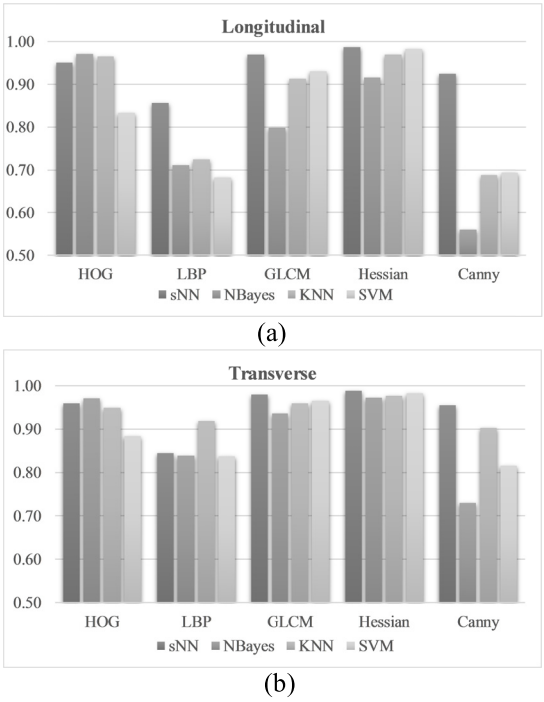

FIGURE 6. Performance comparison of the four classifiers.

E. COMPARISON OF A SHALLOW NEURAL NETWORK WITH THE THREE CLASSIFIERS

The four classifiers were sNN, NBayes, KNN and SVM. The shallow neural network (sNN) was a seven-layer neural network with four completely-coupled nodes. The detailed definition may be found in this section. The vertical axis was the prediction accuracy of a classification model. Each of the five feature types extracted from the longitudinal or transverse ultrasonograms was evaluated for its prediction performance with one of the four classifiers.

The shallow completely-joined neural network (sNN) was constructed from the sequential model. This model has seven layers, *i.e.*, four layers of completely-coupled nodes and three interface layers (two dropout layer and one completely connected layer), all of which utilized the relu activation functions and its dropout parameter was 0.3. This classifier was denoted as sNN.

The classifier sNN achieved the best TPC prediction accuracies on both longitudinal and transverse views of the ultrasonograms, as shown in Figure 6. The best longitudinal model of sNN achieved the accuracy Acc = 0.9876, while the best transverse model achieved Acc = 0.9885. Both of the two best models were based on the Hessian features, suggesting that the Hessian features may extract essential information from the biomedical ultrasonograms [62], [63]. This observation was further supported by that the second best models of both the longitudinal and transverse views were trained by the same classifier SVM on the Hessian features, as shown in Figure 6. And the overall best model was achieved by the classifier sNN with the Hessian features.

F. TWO FEATURES TYPES ARE BETTER THAN ONE BASED ON NEURAL NETWORKS

Each grid was the best 5-fold cross validation accuracy of a classifier C using two types of features (AlgA, AlgB) of either longitudinal or transverse ultrasonograms. AlgA or AlgB could be one of the five feature types, i.e., HOG, LBP, GLCM, Hessian and Canny. The accuracy in the upper triangle was calculated by combining the features of AlgA and AlgB and then selecting features with GBDT. This feature selection strategy was denoted as C-FS. The accuracy in the lower triangle was calculated by selecting features in AlgA and AlgB separately and then combining the selected features. This was denoted as the FS-C feature selection strategy. The classifier C was the shallow neural network with hidden layers of fully connected nodes.

The SVM model performed the best (Acc = 0.9828) using a single feature type Hessian in the previous sections and may be improved by integrating other feature types, as shown in Figure 7. This best model based on one feature type was improved by at least 0.0058 in accuracy by the Canny features. And the best model based on two feature types achieved Acc = 0.9943 by integrating the GLCM and Hessian features. Figure 7 also demonstrated that a better prediction accuracy may be achieved by selecting features for each feature type and then integrating the chosen features (FS + C strategy), compared with the strategy of selecting features after combining two feature types (C + FS strategy). And the Hessian features collaborated well with the other feature types, with an improved prediction accuracy when being integrated with any of the other four feature types.

C-FS							
HOG							0.9943
LBP	0.9794						0.9656
GLCM	0.9886	0.9726					0.6625
Hessian	0.9888	0.9914	0.9886				
Canny	0.9785	0.6625	0.9768	0.9886			
	HOG	LBP	GLCM	Hessian	Canny		
Canny	0.9771	0.9686	0.9654	0.9886			
Hessian	0.9920	0.9920	0.9943				
GLCM	0.9714	0.9714					
LBP	0.9753						
HOG							
FS-C							

FIGURE 7. Duet heatmap of the five feature types.

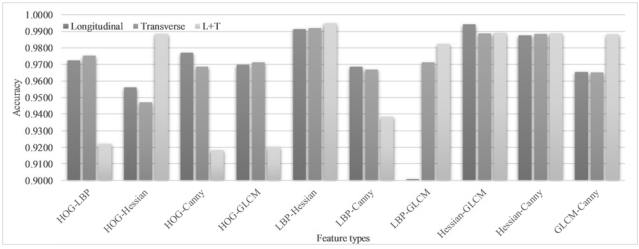

FIGURE 8. Multi-view integrated prediction of TPC.

It's interesting to observe that one feature type could always be improved by integrating other feature types, but it's important to select a good collaborator, as shown in Figure 7. For example, only 0.9714 in Acc was achieved by integrating the HOG and GLCM features, while the HOG features alone generated a model with Acc = 0.9717.

G. INTEGRATING BOTH VIEWS OF ULTRASONOGRAMS

Each column was the TPC prediction accuracy calculated by integrating two feature types with the FS + C strategy. The data series "Longitudinal", "Transverse" and "L + T" were based on the longitudinal, transverse and both views of the ultrasonograms.

The feature type Hessian represented the best information source for the TPC prediction, as shown in Figure 8. Three of the four best models were achieved by the two feature types Hessian and LBP, and the integration of the two ultrasonogram views (Acc = 0.9949) outperformed either view alone. Except for the integration of the LBP and GLCM features using two ultrasonogram views (Acc = 0.9823), all the other models using the LBP features performed worse than 0.9800 in Acc. Actually the LBP features achieved Acc = 0.9183, only better than the Canny features with Acc = 0.9022, as shown in Figures 2 and 3.

So the best TPC prediction model was achieved using the Hessian and LBP features of both ultrasonogram views. The features were selected by the FS + C strategy and the prediction accuracy was Acc = 0.9949.

Uliyan, DM et al., demonstrated that a combination of LBP and Hessian features performed very well on the biomedical image-based classification problem [64]. Figure 1 suggested that LBP and Hessian had the largest averaged values among the five feature types. Our comprehensive evaluation of all the duets of feature types also supported that the integration of LBP and Hessian feature types achieved the best prediction performances, as shown in Figure 8.

IV. CONCLUSION AND FUTURE SCOPES

This study investigated the ultrasonogram-based thyroid papillary carcinoma (TPC) prediction problem. Five popular types of features were extracted from the two ultrasonogram views, i.e., longitudinal and transverse. The best model achieved the prediction accuracy 0.9949 using the LBP and Hessian features extracted from both longitudinal and transverse views of the ultrasonograms.

An integrated model of two feature types tended to outperform the models using only one feature type. The Hessian features outperformed any one of the other four feature types, and the Hessian-based model may be further improved by integrating one more feature type.

ACKNOWLEDGMENTS

Constructive comments from the anonymous reviewers were greatly appreciated.

REFERENCES

[1] B. Kim, "Thyroid hormone as a determinant of energy expenditure and the basal metabolic rate," *Thyroid*, vol. 18, no. 2, pp. 141–144, Feb. 2008.
[2] J. Calonne, L. Isacco, J. Miles-Chan, D. Arsenijevic, J.-P. Montani, C. Guillet, Y. Boirie, and A. G. Dulloo, "Reduced skeletal muscle protein turnover and thyroid hormone metabolism in adaptive thermogenesis that facilitates body fat recovery during weight regain," *Frontiers Endocrinol.*, vol. 10, p. 119, Feb. 2019.
[3] W. M. Wiersinga, "Graves' disease: Can it be cured?" *Endocrinol. Metabolism*, vol. 34, no. 1, pp. 29–38, Mar. 2019.
[4] S. Malmstroem, D. Grove-Laugesen, A. L. Riis, B. J. Bruun, E. Ebbehoj, K. W. Hansen, T. Watt, and L. Rejnmark, "Muscle performance and postural stability are reduced in patients with newly diagnosed graves' disease," *Thyroid*, vol. 29, no. 6, pp. 783–789, Apr. 2019.
[5] T. Carling and R. Udelsman, "Thyroid cancer," *Annu. Rev. Med.*, vol. 65, pp. 125–137, Jan. 2014.
[6] N. Oishi, T. Kondo, A. Ebina, Y. Sato, J. Akaishi, R. Hino, N. Yamamoto, K. Mochizuki, T. Nakazawa, H. Yokomichi, K. Ito, Y. Ishikawa, and R. Katoh, "Molecular alterations of coexisting thyroid papillary carcinoma and anaplastic carcinoma: Identification of TERT mutation as an independent risk factor for transformation," *Mod. Pathol.*, vol. 30, no. 11, pp. 1527–1537, Nov. 2017.
[7] C. Hedman, T. Djärv, P. Strang, and C. I. Lundgren, "Effect of thyroid-related symptoms on long-term quality of life in patients with differentiated thyroid carcinoma: A population-based study in Sweden," *Thyroid*, vol. 27, no. 8, pp. 1034–1042, Aug. 2017.
[8] A. H. Ellenberg, L. Goldman, G. S. Gordan, and S. J. S. Lindsay, "Thyroid carcinoma in patients with hyperparathyroidism," *Surgery*, vol. 51, no. 6, pp. 708–717, 1962.
[9] B. Abboud, T. Smayra, H. Jabbour, C. Ghorra, and G. Abadjian, "Correlations of neck ultrasound and pathology in cervical lymph node of papillary thyroid carcinoma," *Acta Chirurgica Belgica*, to be published.
[10] S. Liu, C. Xu, Y. Zhang, J. Liu, B. Yu, X. Liu, and M. Dehmer, "Feature selection of gene expression data for cancer classification using double RBF-kernels," *BMC Bioinf.*, vol. 19, Oct. 2018, Art. no. 396.
[11] G. H. Tan and H. Gharib, "Thyroid incidentalomas: Management approaches to nonpalpable nodules discovered incidentally on thyroid imaging," *Ann. Internal Med.*, vol. 126, no. 3, pp. 31–226, Feb. 1997.
[12] S. J. Mandel, "A 64-year-old woman with a thyroid nodule," *JAMA*, vol. 292, no. 21, pp. 2632–2642, Dec. 2004.
[13] L. Hegedüs, "Clinical practice. The thyroid nodule," *New England J. Med.*, vol. 351, pp. 1764–1771, Oct. 2004.

[14] D. S. Cooper, G. M. Doherty, B. R. Haugen, R. T. Kloos, S. L. Lee, S. J. Mandel, E. L. Mazzaferri, B. McIver, F. Pacini, M. Schlumberger, S. I. Sherman, D. L. Steward, and R. M. Tuttle, "Revised American thyroid association management guidelines for patients with thyroid nodules and differentiated thyroid cancer: The American thyroid association (ATA) guidelines taskforce on thyroid nodules and differentiated thyroid cancer," *Thyroid*, vol. 19, no. 11, pp. 214–1167, Nov. 2009.

[15] J. P. Brito, M. R. Gionfriddo, A. Al Nofal, K. R. Boehmer, A. L. Leppin, C. Reading, M. Callstrom, T. A. Elraiyah, L. J. Prokop, M. N. Stan, M. H. Murad, J. C. Morris, and V. M. Montori, "The accuracy of thyroid nodule ultrasound to predict thyroid cancer: Systematic review and meta-analysis," *J. Clin. Endocrinol. Metabolism*, vol. 99, no. 4, pp. 63–1253, Apr. 2014.

[16] Q. Zheng, S. L. Furth, G. E. Tasian, and Y. Fan, "Computer-aided diagnosis of congenital abnormalities of the kidney and urinary tract in children based on ultrasound imaging data by integrating texture image features and deep transfer learning image features," *J. Pediatric Urol.*, vol. 15, no. 1, pp. 75-e1–75-e7, Feb. 2019.

[17] U. R. Acharya, K. M. Meiburger, J. E. W. Koh, E. J. Ciaccio, N. Arunkumar, M. H. See, N. A. M. Taib, A. Vijayananthan, K. Rahmat, F. Fadzli, S. S. Leong, C. J. Westerhout, A. Chantre-Astaiza, and G. Ramirez-Gonzalez, "A novel algorithm for breast lesion detection using textons and local configuration pattern features with ultrasound imagery," *IEEE Access*, vol. 7, pp. 22829–22842, 2019.

[18] S. Sasikala, M. Ezhilarasi, and S. Senthil, "Breast cancer diagnosis system based on the fusion of local binary and ternary patterns from ultrasound B mode and elastography images," *Current Med. Imag. Rev.*, vol. 14, no. 6, pp. 947–956, 2018.

[19] N. A. Shaharuddin and W. M. H. W. Mahmud, "Feature analysis of kidney ultrasound image in four different ultrasound using gray level co-occurrence matrix (GLCM) and intensity histogram (IH)," *Int. J. Integr. Eng.*, vol. 10, no. 3, pp. 42–47, 2018.

[20] H. Yang, A. Pourtaherian, C. Shan, and A. F. Kolen, "Feature study on catheter detection in three-dimensional ultrasound," *Proc. SPIE*, vol. 10576, Mar. 2018, Art. no. 105760V.

[21] H. Li, J. Weng, Y. Shi, W. Gu, Y. Mao, Y. Wang, W. Liu, and J. Zhang, "An improved deep learning approach for detection of thyroid papillary cancer in ultrasound images," *Sci. Rep.*, vol. 8, no. 1, Apr. 2018, Art. no. 6600.

[22] C. Carmeci, R. B. Jeffrey, I. R. McDougall, K. W. Nowels, and R. J. Weigel, "Ultrasound-guided fine-needle aspiration biopsy of thyroid masses," *Thyroid*, vol. 8, no. 4, pp. 283–289, Apr. 1998.

[23] G. Taherzadeh, A. Dehzangi, M. Golchin, Y. Zhou, and M. P. Campbell, "SPRINT-Gly: Predicting N- and O-linked glycosylation sites of human and mouse proteins by using sequence and predicted structural properties," *Bioinformatics*, to be published.

[24] M. Wiercioch, "Exploring the potential of spherical harmonics and PCVM for compounds activity prediction," *Int. J. Mol. Sci.*, vol. 20, no. 9, p. 2175, May 2019.

[25] K. Li, S. Wang, C. Du, Y. Huang, X. Feng, and F. Zhou, "Accurate fatigue detection based on multiple facial morphological features," *J. Sensors*, vol. 2019, Feb. 2019, Art. no. 7934516.

[26] C. Xu, J. Liu, W. Yang, Y. Shu, Z. Wei, W. Zheng, X. Feng, and F. Zhou, "An OMIC biomarker detection algorithm TriVote and its application in methylomic biomarker detection," *Epigenomics*, vol. 10, no. 4, pp. 335–347, Apr. 2018.

[27] R. Ge, M. Zhou, Y. Luo, Q. Meng, G. Mai, D. Ma, G. Wang, and F. Zhou, "McTwo: A two-step feature selection algorithm based on maximal information coefficient," *BMC Bioinf.*, vol. 17, no. 1, p. 142, 2016.

[28] K. E. Richardson and B. M. Znosko, "Nearest-neighbor parameters for 7-deaza-adenosineÂů uridine base pairs in RNA duplexes," *RNA*, vol. 22, no. 6, pp. 934–942, Jun. 2016.

[29] A. D. Rodgers, H. Zhu, D. Fourches, I. Rusyn, and A. Tropsha, "Modeling liver-related adverse effects of drugs using kNearest neighbor quantitative structure-activity relationship method," *Chem. Res. Toxicol.*, vol. 23, no. 4, pp. 32–724, Apr. 2010.

[30] W. Sun, C. Chang, Y. Zhao, and Q. Long, "Knowledge-guided Bayesian support vector machine for high-dimensional data with application to analysis of genomics data," in *Proc. IEEE Int. Conf. Big Data*, Dec. 2018, pp. 1484–1493.

[31] M. Wang, C. Li, W. Zhang, Y. Wang, Y. Feng, Y. Liang, J. Wei, X. Zhang, X. Li, and R. Chen, "Support vector machine for analyzing contributions of brain regions during task-state fMRI," *Frontiers Neuroinf.*, vol. 13, p. 10, Mar. 2019.

[32] A. Jalalian, S. Mashohor, R. Mahmud, B. Karasfi, M. I. B. Saripan, and A. R. B. Ramli, "Foundation and methodologies in computer-aided diagnosis systems for breast cancer detection," *EXCLI J.*, vol. 16, pp. 113–137, Feb. 2017.

[33] V. K. Sudarshan, "Application of wavelet techniques for cancer diagnosis using ultrasound images: A review," *Comput. Biol. Med.*, vol. 69, pp. 97–111, Feb. 2016.

[34] N. Dalal and B. Triggs, "Histograms of oriented gradients for human detection," in *Proc. Int. Conf. Comput. Vis. Pattern Recognit. (CVPR)*, vol. 1, Jun. 2005, pp. 886–893.

[35] F. Suard, A. Rakotomamonjy, A. Bensrhair, and A. Broggi, "Pedestrian detection using infrared images and histograms of oriented gradients," in *Proc. IEEE Intell. Vehicles Symp.*, Jun. 2006, pp. 206–212.

[36] E. Adetiba and O. O. Olugbara, "Lung cancer prediction using neural network ensemble with histogram of oriented gradient genomic features," *Sci. World J.*, vol. 2015, Jan. 2015, Art. no. 786013.

[37] D. Unay, A. Ekin, M. Cetin, R. Jasinschi, and A. Ercil, "Robustness of local binary patterns in brain MR image analysis," in *Proc. 29th Annu. IEEE Int. Conf. Eng. Med. Biol. Soc. (EMBS)*, Aug. 2007, pp. 2098–2101.

[38] L. Nanni, A. Lumini, and S. Brahnam, "Local binary patterns variants as texture descriptors for medical image analysis," *Artif. Intell. Med.*, vol. 49, no. 2, pp. 117–125, 2010.

[39] D.-C. He and L. Wang, "Texture unit, texture spectrum, and texture analysis," *IEEE Trans. Geosci. Remote Sens.*, vol. 28, no. 4, pp. 509–512, Jul. 1990.

[40] L. Wang and D.-C. He, "Texture classification using texture spectrum," *Pattern Recognit.*, vol. 23, no. 8, pp. 905–910, 1990.

[41] T. Ahonen, A. Hadid, and M. Pietikainen, "Face description with local binary patterns: Application to face recognition," *IEEE Trans. Pattern Anal. Mach. Intell.*, vol. 28, no. 12, pp. 2037–2041, Dec. 2006.

[42] T. Ahonen, J. Matas, C. He, and M. Pietikäinen, "Rotation invariant image description with local binary pattern histogram Fourier features," in *Proc. Scandin. Conf. Image Anal.* Oslo, Norway: Springer, 2009, pp. 61–70.

[43] G. Zhao, T. Ahonen, J. Matas, and M. Pietikäinen, "Rotation-invariant image and video description with local binary pattern features," *IEEE Trans. Image Process.*, vol. 21, no. 4, pp. 1465–1477, Apr. 2012.

[44] X. Wang, T. X. Han, and S. Yan, "An HOG-LBP human detector with partial occlusion handling," in *Proc. IEEE 12th Int. Conf. Comput. Vis.*, Sep. 2009, pp. 32–39.

[45] C. Silva, T. Bouwmans, and C. Frélicot, "An extended center-symmetric local binary pattern for background modeling and subtraction in videos," in *Proc. Int. Joint Conf. Comput. Vis., Imag. Comput. Graph. Theory Appl. (VISAPP)*, 2015, pp. 1–9.

[46] W. Gomez, W. C. A. Pereira, and A. F. C. Infantosi, "Analysis of co-occurrence texture statistics as a function of gray-level quantization for classifying breast ultrasound," *IEEE Trans. Med. Imag.*, vol. 31, no. 10, pp. 1889–1899, Oct. 2012.

[47] N. Fujima, A. Homma, T. Harada, Y. Shimizu, K. K. Tha, S. Kano, T. Mizumachi, R. Li, K. Kudo, and H. Shirato, "The utility of MRI histogram and texture analysis for the prediction of histological diagnosis in head and neck malignancies," *Cancer Imag.*, vol. 19, no. 1, p. 5, Feb. 2019.

[48] P. Yin, N. Mao, C. Zhao, J. Wu, L. Chen, and N. Hong, "A triple-classification radiomics model for the differentiation of primary chordoma, giant cell tumor, and metastatic tumor of sacrum based on T2-weighted and contrast-enhanced T1-weighted MRI," *J. Magn. Reson. Imag.*, vol. 49, no. 3, pp. 752–759, Mar. 2019.

[49] Y. N. Hwang, J. H. Lee, G. Y. Kim, E. S. Shin, and S. M. Kim, "Characterization of coronary plaque regions in intravascular ultrasound images using a hybrid ensemble classifier," *Comput. Methods Programs Biomed.*, vol. 153, pp. 83–92, Jan. 2018.

[50] P. P. R. Filho, R. M. Sarmento, G. B. Holanda, and D. De Alencar Lima, "New approach to detect and classify stroke in skull CT images via analysis of brain tissue densities," *Comput. Methods Programs Biomed.*, vol. 148, pp. 27–43, Sep. 2017.

[51] M. C. Bartholomew-Biggs, "The estimation of the Hessian matrix in non-linear least squares problems with non-zero residuals," *Math. Program.*, vol. 12, no. 1, pp. 67-80, 1977.

[52] H. Zhao, G. Wang, R. Lin, X. Gong, L. Song, T. Li, W. Wang, K. Zhang, X. Qian, H. Zhang, and L. Li, "Three-dimensional Hessian matrix-based quantitative vascular imaging of rat iris with optical-resolution photoacoustic microscopy *in vivo*," *J. Biomed. Opt.*, vol. 23, no. 4, Apr. 2018, Art. no. 046006.

[53] B. Thangaraju, I. Vennila, and G. Chinnasamy, "Detection of microcalcification clusters using Hessian matrix and foveal segmentation method on multiscale analysis in digital mammograms," *J. Digit. Imag.*, vol. 25, no. 5, pp. 607–619, Oct. 2012.
[54] C.-X. Deng, G.-B. Wang, and X.-R. Yang, "Image edge detection algorithm based on improved canny operator," in *Proc. Int. Conf. Wavelet Anal. Pattern Recognit.*, Jul. 2013, pp. 168–172.
[55] Y.-K. Huo, G. Wei, Y.-D. Zhang, and L.-N. Wu, "An adaptive threshold for the canny operator of edge detection," in *Proc. Int. Conf. Image Anal. Signal Process.*, Apr. 2010, pp. 371–374.
[56] X.-Q. Zeng and G.-Z. Li, "Supervised redundant feature detection for tumor classification," *BMC Med. Genomics*, vol. 7, no. 2, p. S5, 2014.
[57] J. Elith, J. R. Leathwick, and T. Hastie, "A working guide to boosted regression trees," *J. Animal Ecol.*, vol. 77, no. 4, pp. 802–813, Jul. 2008.
[58] D. Cossock and T. Zhang, "Statistical analysis of Bayes optimal subset ranking," *IEEE Trans. Inform. Theory*, vol. 54, no. 11, pp. 5140–5154, Nov. 2008.
[59] H. Zhang, A. C. Berg, M. Maire, and J. Malik, "SVM-KNN: Discriminative nearest neighbor classification for visual category recognition," in *Proc. IEEE Comput. Soc. Conf. Comput. Vis. Pattern Recognit. (CVPR)*, vol. 2, Jun. 2006, pp. 2126–2136.
[60] Y. LeCun, L. Bottou, Y. Bengio, and P. Haffner, "Gradient-based learning applied to document recognition," *Proc. IEEE*, vol. 86, no. 11, pp. 2278–2324, Nov. 1998.
[61] Z.-W. Yuan and J. Zhang, "Feature extraction and image retrieval based on AlexNet," in *Proc. 8th Int. Conf. Digit. Image Process. (ICDIP)*, vol. 10033, 2016, Art. no. 100330E.
[62] M. Bayat, M. Fatemi, and A. Alizad, "Background removal and vessel filtering of noncontrast ultrasound images of microvasculature," *IEEE Trans. Biomed. Eng.*, vol. 66, no. 3, pp. 831–842, Mar. 2019.
[63] Z. Fanti, F. Torres, E. Hazan-Lasri, A. Gastelum-Strozzi, L. Ruiz-Huerta, A. Caballero-Ruiz, and F. A. Cosío, "Improved surface-based registration of CT and intraoperative 3D ultrasound of bones," *J. Healthcare Eng.*, vol. 2018, Jun. 2018, Art. no. 2365178.
[64] D. M. Uliyan, H. A. Jalab, and A. W. A. Wahab, "Copy move image forgery detection using Hessian and center symmetric local binary pattern," in *Proc. IEEE Conf. Open Syst. (ICOS)*, Aug. 2015, pp. 7–11.

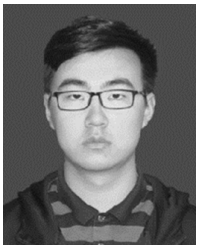

RENXIANG ZHU is currently pursuing the degree through the Tang Aoqing Honors Program (computer science) with the College of Computer Science and Technology, Jilin University, Changchun, China. His research interests include computer vision, natural language processing, and intelligent control robot and bioinformatics.

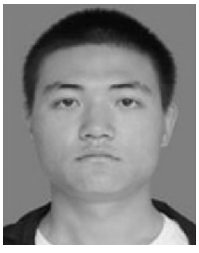

ZHONGYU WANG is currently pursuing the bachelor's degree with the College of Computer Science and Technology, Jilin University, Jilin, China. He is a member of the Tang Aoqing Honors Program in Science. He joined the HILab in the first year of college.

YIFAN ZHANG is currently pursuing the bachelor's degree with the College of Computer Science and Technology, Jilin University, Jilin, China. His research interests include NLP and image recognition.

BINGXIN YU received the master's degree from the College of Clinical Medicine, Jilin University, Changchun, China, in 2012. In 2012, she began to work with the Ultrasound Department, China-Japan Union Hospital, Jilin University. She is currently pursuing the Ph.D. degree with the Key Laboratory of Zoonosis, Department of Pathogenobiology, College of Basic Medicine, Ministry of Education of China, Jilin University, Changchun. Her research interests include ultrasonic information sciences and medical image processing.

MINGRAN QI received the B.Sc. degree from the College of Clinical Medicine, Jilin University, Changchun, China, in 2016. She is currently pursuing the Ph.D. degree with the Key Laboratory of Zoonosis, Department of Pathogenobiology, College of Basic Medicine, Ministry of Education of China, Jilin University, Changchun. Her research interests include genomics and the non-coding RNA of gastric cancer.

XIN FENG received the master's degree from the School of Software, Jilin University, in 2013. In 2016, she went to the School of Computer Science, Jilin University, to pursue the Ph.D. degree. She is mainly devoted to the research of biomedical big data during the reading period.

CHENJUN WU is currently pursuing the bachelor's degree with the College of Computer Science and Technology, Jilin University, Jilin, China. Her research interests include NLP and CV.

YUXUAN CUI is pursuing the bachelor's degree with the College of Computer Science and Technology, Jilin University, Jilin, China. His research interest includes data analysis.

FAN LI is currently a Professor and a Doctoral Supervisor. She is currently pursuing the Doctor of Medicine degree. Her research interests include the new detection technology of pathogens, the occurrence and transmission mechanism of bacterial drug resistance, virology, biological materials, medical imaging informatics, and other fields.

LAN HUANG received the Ph.D. degree from the College of Computer Science and Technology, Jilin University, Changchun, China, in 2003, where she is currently a Professor with the College of Computer Science and Technology. Her research interests include data mining and business intelligence.

FENGFENG ZHOU received the bachelor's and Ph.D. degrees in computer sciences from the University of Science and Technology of China, in 2000 and 2005, respectively. His Lab at the Jilin University focuses on the development of feature selection algorithms for biomedical big data.